J. Fluid Mech. (2002), *vol.* 452, *pp.* 303–323.
DOI: 10.1017/S0022112001006747 Printed in the United Kingdom

Instability of a bed of particles sheared by a viscous flow

By FRANÇOIS CHARRU
AND HÉLÈNE MOUILLERON-ARNOULD

Institut de Mécanique des Fluides de Toulouse, 2, allée du Professeur C. Soula, 31400 Toulouse, France

(Received 5 January 2001 and in revised form 6 August 2001)

The instability of a bed of particles sheared by a viscous fluid is investigated theoretically. The viscous flow over the wavy bed is first calculated, and the bed shear stress is derived. The particle transport rate induced by this bed shear stress is calculated from the viscous resuspension theory of Leighton & Acrivos (1986). Mass conservation of the particles then gives explicit expressions for the wave velocity and growth rate, which depend on four dimensionless parameters: the wavenumber, the fluid thickness, a viscous length and the shear stress. The mechanism of the instability is given. It appears that for high enough fluid-layer thickness, long-wave instability arises as soon as grains move, while short waves are stabilized by gravity. For smaller fluid thickness, the destabilizing effect of fluid inertia is reduced, so that the moving flat bed is stable for small shear stress, and unstable for high shear stress. The most amplified wavelength scales with the viscous length, in agreement with the few available experiments for small particle Reynolds numbers. The results are also compared with related studies for turbulent flow.

1. Introduction

When an initially flat bed of small heavy particles is sheared by a clear fluid, the bed is unstable and ripples grow. Such flows, which are encountered in many industrial applications and in the natural environment, can be either oscillating or steady. Sand ripples observed in shallow water along beaches correspond to the oscillating case, the oscillating flow near the bed being created by surface waves (Blondeaux 1990). Ripples observed in rivers or in closed or open channels correspond to the steady case; here, small deformations of the upper fluid surface do not couple with the bed, so long as the flow depth is great enough. This paper is devoted to the latter case of ripple formation under steady flow; more precisely, we show, on the basis of a simple analytical model, that a viscous shear flow may be responsible for the bed instability.

Sheared beds of particles have been studied within two different contexts, chemical engineering and hydraulic engineering. Within the former context, the resuspension of small particles due to hydrodynamic interactions was first studied by Gadala-Maria & Acrivos (1980). For vanishing particle Reynolds number, the height of the resuspended layer grows linearly with the shear stress, and is typically a few particle diameters thick for moderate shear stress (Leighton & Acrivos 1986). The stability of such resuspension flows has not been studied extensively. However, several Poiseuille flow experiments show the appearance of waves at the interface between the

resuspended layer and the clear fluid (Kuru, Leighton & McCready 1995; Schaflinger 1994; Schaflinger, Acrivos & Stibi 1995; Schaflinger, Acrivos & Zhang 1990).

The existing stability analyses consider the resuspended layer as an effective Newtonian fluid whose viscosity and density depend on the local particle concentration ϕ. Zhang, Acrivos & Schaflinger (1992) consider the particle layer as a well-mixed suspension with uniform particle concentration ϕ, so that the base flow is a two-layer plane Poiseuille flow. Accordingly, they recover the long- and short-wave instabilities due to the jump in viscosity discovered by Yih (1967) and Hooper & Boyd (1983), respectively. The long-wave analysis of Loimer & Schaflinger (1998) introduces corrections of the viscosity and density with the interface height, which ensure mass conservation of the particles, and also includes a slip velocity of the suspended layer at the bottom wall. This improvement leads to an additional instability for small thickness of the less viscous clear fluid, which is not present in two-layer flows. In the studies of Zhang *et al.* and Loimer & Schaflinger, the assumption of uniform particle concentration implies a parabolic velocity profile with negative curvature in both layers, and a discontinuous slope of the velocity profile at the interface due to the viscosity jump. This assumption greatly simplifies the analysis, and may be valid far from the threshold of particle movement (high Shields number) where the whole layer is resuspended. However, this assumption is not valid for smaller shear rates where the particle concentration varies continuously within the resuspended layer. Indeed, the effective viscosity gradient leads to a change of curvature of the velocity profile at the interface, which can be expected to affect the stability of the flow.

Miskin, Elliott & Ingham (1999) take into account the velocity profile of the resuspended layer, as calculated by Schaflinger *et al.* (1990). However, the particle concentration is not perturbed in this study, which is a questionable assumption. This analysis amounts to solving the Orr–Sommerfeld equation for channel flow, with given profiles for the basic streamfunction, density and viscosity. Long waves are found to be always unstable, with the striking result that the wavenumber $k = 0$ is generally unstable (whereas it might be expected to be neutral) and that it is the most unstable wavenumber for small Reynolds numbers. For completeness, it should be noted that the simulations by Stokesian dynamics of Morris & Brady (1998) do not report instabilities.

Within the context of hydraulic engineering, the stability of a bed of particles is related to the formation of sediment ripples by river or coastal currents (Raudkivi 1998). Despite the huge number of experimental and theoretical studies, this problem is not well understood and even the relevance of stability analyses is questioned (Raudkivi 1997). The methodology of the available stability analyses is as follows. Velocities in the moving bed are assumed small compared to those of the clear fluid, so that the turbulent flow above a sinusoidal bed disturbance is calculated as if the bed were fixed. The bed shear stress is then derived, and semi-empirical laws then give the corresponding perturbed particle transport rate. Mass conservation in the moving bed finally gives the growth rate of the instability. The most amplified wavelengths predicted by such stability calculations (Engelund & Fredsøe 1982; Richards 1980; Sumer & Bakioglu 1984) agree with the observed ripple length in some experiments in a particular range of particle Reynolds numbers, e.g. those of Coleman & Melville (1996), but the predicted wavelengths are much shorter than those observed in most other experiments (Yalin 1985). Part of the discrepancy may arise from the parametrization of the turbulence. Therefore, as pointed out earlier by Bagnold (1966), investigation of viscous flows may improve our understanding of the problem and the physical mechanisms involved. Indeed, some experiments with small

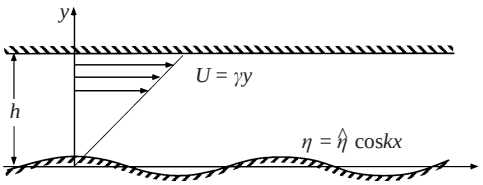

FIGURE 1. Couette flow over a wavy bed.

non-cohesive particles performed by Mantz (1978) show that ripples grow within the viscous sublayer, even when particle inertia is small.

The present paper thus addresses the question of the instability of a bed of particles under a viscous linear shear flow. Particles are assumed non-cohesive, with diameters much greater than 1 μm so that Brownian motion can be neglected. The methodology parallels the 'quasi-static' methodology sketched above for a sand bed sheared by turbulent water. The perturbed flow over a small-amplitude sinusoidal disturbance is first calculated as if the bed were fixed, and the bed shear stress is derived (§ 2). The particle flow rate driven by the bed shear stress is then calculated from the viscous resuspension theory of Leighton & Acrivos (1986) (§ 3). The particle mass conservation equation finally gives the wave velocity and growth rate of the disturbance (§ 4). The results are discussed in the final section, with emphasis on the validity of the hypotheses involved in the model, on the physical mechanism of the instability, and on a comparison with other studies (§ 5).

2. Flow over a sinusoidal fixed bed

In this section, we consider the linear shear flow over a fixed sinusoidal bed, $\eta = \hat{\eta}\cos kx$ (figure 1). From the results of Charru & Hinch (2000), we show that the bed shear stress disturbance is not in phase with the bed disturbance, owing to inertia effects. It will be shown in § 4 that this inertia-induced phase lag is responsible for the bed instability. The problem involves three length scales, namely the inverse wavenumber k^{-1}, the thickness h, and the viscous length $l_v = (\nu/k\gamma)^{1/3}$, where ν is the kinematic fluid viscosity and γ the shear rate. Taking k^{-1} as the unit length, the problem therefore depends on two parameters, the dimensionless thickness kh and dimensionless viscous length kl_v. For future convenience we also introduce the shear Reynolds number Re:

$$Re := \frac{\gamma h^2}{\nu} = \frac{(kh)^2}{(kl_v)^3}. \tag{1}$$

The flow can be considered as the sum of a basic flow $U = \gamma y$ over a flat bed ($\hat{\eta} = 0$), and disturbances $(u, v) = \frac{1}{2}(\hat{u}(y), \hat{v}(y))\exp(\mathrm{i}kx) + \text{c.c.}$ induced by the bed disturbance. For small bed slopes, i.e. $k\hat{\eta} \ll 1$, the linearized vorticity equation can be recast into the standard Airy equation through the change of variable $z(y) = \mathrm{e}^{\mathrm{i}\pi/6}(ky - \mathrm{i}(kl_v)^3)/kl_v$. The amplitude of the vorticity disturbance $\omega = \frac{1}{2}\hat{\omega}(y)\exp(\mathrm{i}kx) + \text{c.c.}$ is then given by

$$\frac{\hat{\omega}(y)}{\gamma} = \{C_1(kh, kl_v)\mathrm{Ai}(z(y)) + C_2(kh, kl_v)\mathrm{Bi}(z(y))\}k\hat{\eta}, \tag{2}$$

where Ai and Bi are the Airy functions and C_1 and C_2 are integration constants. Then, the streamfunction ψ can be obtained from the equation $\partial_y^2\hat{\psi} - \hat{\psi} = -\hat{\omega}$, and C_1 and C_2 are determined from the no-slip boundary conditions at the walls (see Appendix A). The amplitude $\hat{\tau}_b$ of the bed shear stress disturbance $\tau_b = \frac{1}{2}\hat{\tau}_b\exp(\mathrm{i}kx) + \text{c.c.}$, which is

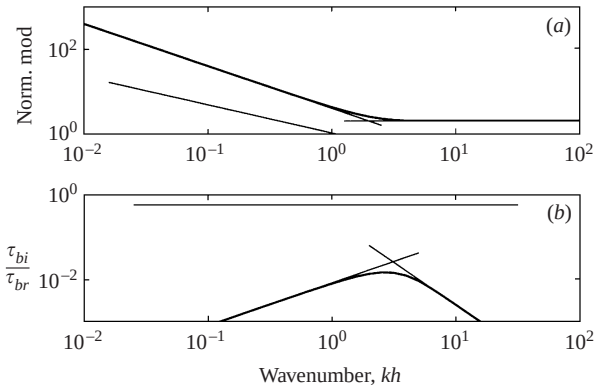

FIGURE 2. Bed shear stress disturbance versus wavenumber kh, for $Re = 1$: (a) normalized modulus $|\hat{\tau}_b|/\mu\gamma k\hat{\eta}$, ($b$) argument $\hat{\tau}_{bi}/\hat{\tau}_{br}$. Straight lines correspond to the asymptotic regimes given by equations (4)–(6).

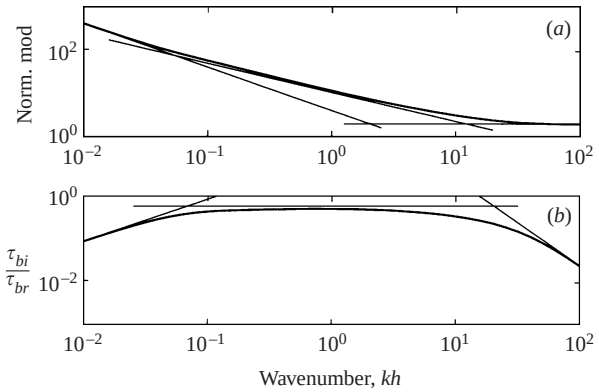

FIGURE 3. As figure 2 but for $Re = 1000$.

the quantity of interest, is then given by

$$\hat{\tau}_b = -\mu\hat{\omega}(0). \tag{3}$$

The origin of the x-axis corresponding to the top of a crest of the bed disturbance ($\eta = \hat{\eta}\cos kx$ with real $\hat{\eta}$), the real part $\hat{\tau}_{br}$ (resp. the imaginary part $\hat{\tau}_{bi}$) of $\hat{\tau}_b$ is the amplitude of the component in phase (resp. out of phase) with the bed disturbance. The phase difference between the bed shear stress τ_b and the bed disturbance η is given by the argument of $\hat{\tau}_b$.

Figures 2 and 3 display the modulus and phase of $\hat{\tau}_b(k)$ normalized by the unperturbed shear stress $\mu\gamma$ and the bed slope $k\hat{\eta}$, for $Re = 1$ and $Re = 1000$, respectively. Straight lines corresponding to asymptotic regimes are also included. For $Re \ll 10$ (figure 2), the asymptotic regimes correspond to $kh \ll 1$ and $kh \gg 1$, and are referred to as the 'shallow viscous' and 'deep viscous' regimes, respectively. The flow in these regimes can be calculated from asymptotic expansions in powers of kh for the shallow viscous regime, and in powers of $(kl_v)^{-3}$ for the deep viscous regime. Then, the following bed shear stress disturbance is obtained:

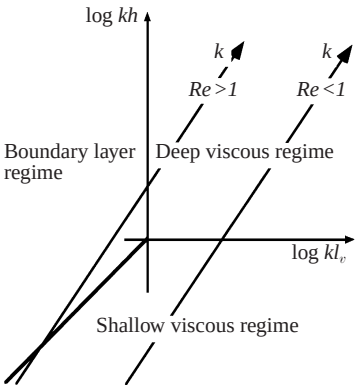

FIGURE 4. Lines of increasing k at constant shear Reynolds number in the (kl_v, kh)-plane for $Re < 1$ and $Re > 1$, and the three asymptotic flow regimes.

shallow viscous regime ($kh \ll 1$)

$$\frac{\hat{\tau}_b}{\mu\gamma} = \left(\frac{4}{kh} + \mathrm{i}\frac{Re}{30}\right) k\hat{\eta}, \tag{4}$$

deep viscous regime ($kh \gg 1$)

$$\frac{\hat{\tau}_b}{\mu\gamma} = \left(2 + \mathrm{i}\frac{1}{2(kl_v)^3}\right) k\hat{\eta}. \tag{5}$$

For $Re \gg 10$ (figure 3), the bed shear stress disturbance for long and short waves is as above, but an intermediate regime appears in the range $Re^{-1} < kh < Re^{1/2}$, referred to as the 'boundary layer' regime. The flow in this regime can be calculated from asymptotic expansions in powers of kl_v, leading to the following bed shear stress disturbance:

boundary layer regime ($Re^{-1} < kh < Re^{1/2}$)

$$\frac{\hat{\tau}_b}{\mu\gamma} = 1.06\mathrm{e}^{\mathrm{i}\pi/6}\frac{1}{kl_v} k\hat{\eta}. \tag{6}$$

Note that in the case of an unbounded flow ($kh = \infty$), the shallow viscous regime simply disappears.

The three flow regimes defined above can be conveniently represented in a 'phase diagram' in the $(\log kl_v, \log kh)$-plane (figure 4). In this plane, the shallow viscous regime lies in the lower right part ($kh \ll 1$ and $kh \ll kl_v$), the deep viscous regime lies in the upper right part ($kh \gg 1$ and $kl_v \gg 1$), and the boundary layer regime lies in the upper left part ($kl_v \ll 1$ and $kl_v \ll kh$). A given shear Reynolds number $Re = (kh)^2/(kl_v)^3$ corresponds to a line with slope 3/2, along which the wavenumber increases from bottom to top. For $Re < 1$, a constant-Re line is to the right of the point $kh = 1$, $kl_v = 1$ and long waves ($kh \ll 1$) are in the shallow viscous regime while short waves ($kh \gg 1$) are in the deep viscous regime. For $Re > 1$, a constant-Re line is to the left of the point $kh = 1$, $kl_v = 1$ and intermediate wavenumbers such that $Re^{-1} < kh < Re^{1/2}$ are in the boundary layer regime.

The physical significance of the three flow regimes can be understood by considering the penetration height of the vorticity disturbances induced by the wavy bed, and the corresponding inertial effects of the base flow on these disturbances (Charru & Hinch 2000). The no-slip condition at this wavy bed creates a longitudinal velocity

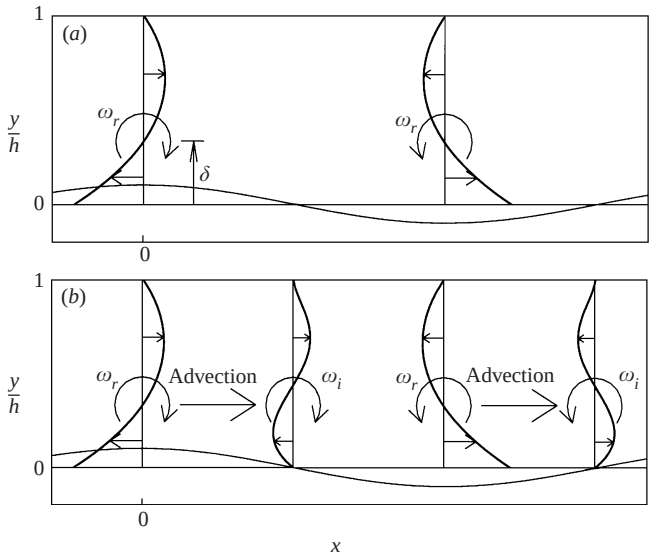

FIGURE 5. (*a*) Typical longitudinal velocity disturbances in phase with the wavy bed, and corresponding vorticity disturbances ω_r and their penetration height δ. (*b*) Same as (*a*) but with the inertially induced out of phase components (the out-of-phase velocity component is magnified by 100 compared to the in-phase component).

disturbance $\hat{u}_r \sim -\gamma\hat{\eta}$, which diffuses over a penetration height δ, and creates a vorticity disturbance $\hat{\omega}_r \sim \hat{u}_r/\delta$ in phase with the bed (figure 5*a*). Asymptotic analysis reveals that the penetration height δ scales with the thickness h when $kh \ll 1$ and $kh \ll kl_v$ (i.e. in the shallow viscous regime), with the inverse wavenumber k^{-1} when $kh \gg 1$ and $kl_v \gg 1$ (i.e. in the deep viscous regime), and with the viscous length l_v when $kl_v \ll 1$ and $kl_v \ll kh$ (i.e. in the boundary layer regime). This implies that in a given regime δ scales with the smallest of the three length scales:

$$\delta \sim \min(k^{-1}, h, l_v), \quad \text{or} \quad k\delta \sim \min(1, kh, kl_v), \tag{7a}$$

and hence the form of the real part of (4)–(6), which corresponds to the component of the shear stress in phase with the wavy bed, $\hat{\tau}_r \sim -\mu\gamma\hat{\eta}/\delta$.

The imaginary part of (4)–(6) corresponds to the shear stress component out of phase with the wavy bed, and arises because of inertia effects. This out-of-phase component can be estimated as follows. As illustrated in figure 5(*b*), advection by the basic flow of the vorticity disturbance $\hat{\omega}_r \sim \hat{u}_r/\delta$ creates an out-of-phase component $\hat{\omega}_i \sim Re_{eff}\hat{\omega}_r$, where Re_{eff} is an effective Reynolds number, which is found from asymptotic analysis to be

$$Re_{eff} \sim \frac{\delta}{l_v}. \tag{7b}$$

Because of the no-slip condition, the out-of-phase velocity disturbance must decrease near the bed. There, the sign of the vorticity disturbance must change, creating an out-of-phase bed shear stress disturbance $\hat{\tau}_{bi} \sim \mu\hat{\omega}_i \sim \mu\gamma Re_{eff}\hat{\eta}/\delta$. For the three flow regimes, the bed shear stress disturbance is shifted upstream by advection, and the maximum phase difference between the shear stress and the wavy bed occurs in the boundary layer regime, where it is close to $\pi/6$. As shown below, the out-of-phase shear stress $\hat{\tau}_{bi}$ is responsible for the instability, because it drags the particles from the troughs to the crests of the bed disturbance.

Ga	$d = 0.090\,\mathrm{mm}$	$d = 0.19\,\mathrm{mm}$	$d = 0.42\,\mathrm{mm}$
$\mu = 10^{-3}\,\mathrm{Pa\,s}$	10	100	1000
$\mu = 10^{-2}\,\mathrm{Pa\,s}$	0.1	1	10
$\mu = 10^{-1}\,\mathrm{Pa\,s}$	0.001	0.01	0.1

TABLE 1. Galileo number for $\rho = 1000\,\mathrm{kg\,m^{-3}}$ and $\rho_p = 2400\,\mathrm{kg\,m^{-3}}$.

3. Particle transport rate

The bed shear stress calculated above slowly drags the particles, and we calculate in this section the resulting particle transport rate. For sand grains sheared by turbulent flow, several semi-empirical laws for the particle transport rate versus the bed shear stress are available, see for example Van Rijn (1993). For viscous flow, Bagnold (1956) was the first to attempt to determine the particle transport rate. However, his result does not exhibit any well-defined interface between the moving bed and the clear fluid: the particle concentration ϕ decreases slowly as $y^{-1/2}$, so that the particle transport rate between the fixed bed and the height y diverges as $\log y$. We use here the viscous resuspension theory of Leighton & Acrivos (1986), according to which particles are lifted up by a shear-induced diffusion mechanism, due to gradients in the particle concentration. This theory, which is summarized in Appendix B, ignores particle inertia, i.e. is valid for very small particle Reynolds number Re_p, defined as

$$Re_p := \frac{\gamma d^2}{\nu} = Re_*^2. \tag{8}$$

(For future use, the above equation also defines the 'turbulent' particle Reynolds number Re_* based on the friction velocity $u_* := (\tau/\rho)^{1/2}$.) Improvements to this theory have been proposed (Phillips *et al.* 1992), but they lead to minor corrections for the flow rate.

3.1. *Particle transport rate for the flat bed*

For viscous flow, the hydrodynamic force acting on a particle with diameter d and density ρ_p is of order $\mu\gamma d^2$, and this force is expected to be of order of the apparent weight $(\rho_p - \rho)gd^3$ of the particle. Thus, the strength of the flow can be measured by the classical Shields number:

$$\Theta = \frac{\mu\gamma}{(\rho_p - \rho)gd}. \tag{9}$$

For future use, we also introduce the Galileo number:

$$Ga := \frac{(\rho_p - \rho)gd^3}{\rho\nu^2} = \frac{(kd)^2}{(kl_v)^3\Theta} = \frac{Re_p}{\Theta}. \tag{10}$$

This number depends on the fluid and particle physical properties only, and it corresponds to (18 times) the sedimentation Reynolds number of a small particle. (Alternatively, $D = Ga^{1/3}$ could be introduced as a dimensionless particle diameter (Raudkivi 1998).) Table 1 shows the range of Ga for typical particle diameters and fluid viscosities. Since Θ is of order one and Re_p must be very small, the Galileo number has to be small too, say $Ga < 1$.

When particles move, the moving bed lies between $y = -h_m$ and $y = 0$ (figure 6). Within this moving bed, the velocity of the mixture increases from zero on the fixed bed to some finite velocity at the interface with the clear fluid, while the volumetric

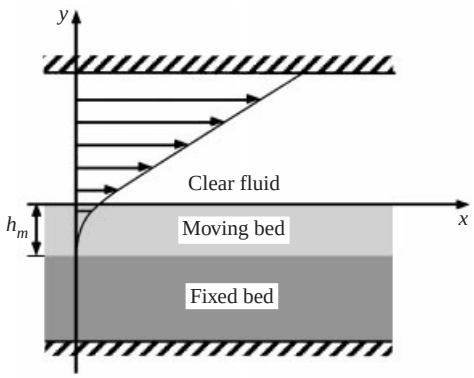

FIGURE 6. Sketch of the Couette resuspension flow.

particle concentration decreases from $\phi_0 \approx 0.58$ to zero. Leighton & Acrivos (1986) found that the thickness of the moving bed increases linearly with the shear stress, according to

$$\frac{h_m}{d} \approx 13.7\Theta. \tag{11}$$

(Note that the numerical constants are very sensitive to ϕ_0: the value $\phi_0 = 0.65$ used by Bagnold leads to $h_m/d \approx 29\Theta$.) Equations (B 5) and (B 6) in Appendix B show that the vertical profiles of the concentration $\phi(y)$ and the velocity $U(y)$ of the mixture can be represented by a single curve when height y and velocity U are normalized by Θd and $\Theta^2 V_S$, respectively, where $V_S = (\rho_p - \rho)gd^2/18\mu$ is the Stokes settling velocity of a single sphere. These normalized profiles are shown in figure 7, together with the relative viscosity profile $\mu_r(\phi)$ ($\mu_r = 1$ for the pure fluid). The particle transport rate can be obtained from

$$Q = \int_{-h_m}^{0} \phi(y)U(y)\,\mathrm{d}y, \tag{12}$$

and is found to be

$$\frac{Q}{V_S d} = C\Theta^3, \quad C \approx 7.5. \tag{13}$$

3.2. *Threshold for particle transport*

It is well-known that settled particles move only if the fluid shear stress exceeds some threshold value. Several studies have been devoted to the determination of the critical fluid conditions for incipient transport of fine grains on a flat bed. For cohesionless sediments, and for 'turbulent' particle Reynolds numbers Re_* smaller than 0.1, the threshold Shields number Θ_t is found to be between 0.17 and 0.26 (Mantz 1977; White 1940; White 1970; Yalin & Karahan 1979). Taking into account the difficulty in defining this threshold, which has been thoroughly discussed by Mantz (1977), we assume in the following that $\Theta_t = 0.2$.

The resuspension theory of Leighton & Acrivos does not take into account the above threshold. Moreover, since this theory considers the moving bed as a continuous medium, it might be valid only when the moving bed is at least a few particle diameters thick. However, experiments (Leighton & Acrivos 1986) showed that the resuspension height grows linearly as predicted by (11), provided that the excess shear stress $(\Theta - \Theta_t)$ is considered, where $\Theta_t \approx 0.26$ is close to the expected threshold for

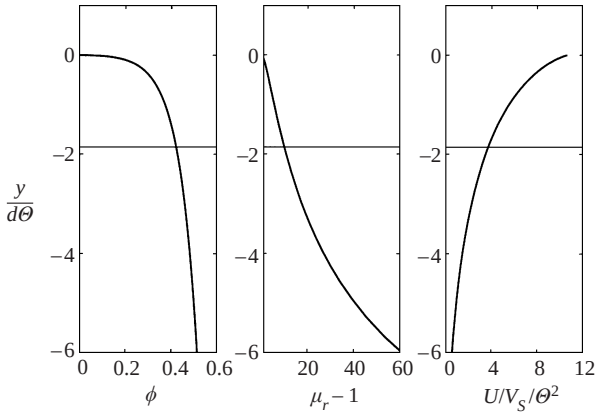

FIGURE 7. Vertical profiles of the concentration ϕ, relative viscosity μ_r and normalized velocity $U/V_S/\Theta^2$, versus the normalized height $y/d/\Theta$. The horizontal line correspond to the interface position at rest, $y/d = -1.86\Theta$.

incipient transport:†

$$\frac{h_m}{d} \approx 13.7(\Theta - \Theta_t). \tag{14}$$

Therefore, we assume that the particle transport rate (13) is modified according to

$$\frac{Q}{V_S d} = C(\Theta - \Theta_t)^3, \quad C = 7.5, \quad \Theta_t = 0.2. \tag{15}$$

Slightly different choices could also be considered and will be addressed in the discussion (§ 5.2). It should be noted that expression (15) agrees with Bagnold (1956), who found $Q \sim (\Theta - \Theta_t)^3$ (multiplied by a diverging logarithmic term as already mentioned). It is also similar to the semi-empirical formulas commonly used in hydraulic engineering, such as the Meyer-Peter & Müller formula $Q \sim (\Theta - \Theta_t)^{3/2}$ (Fredsøe & Deigaard 1992).

3.3. *Particle transport rate disturbance*

Now consider that the moving bed is perturbed sinusoidally on a scale much longer than its thickness ($kh_m \approx 13.7kd\Theta \ll 1$), and calculate the disturbance of the particle transport rate. Let $\eta(x,t) = \frac{1}{2}(\hat{\eta}\exp(\mathrm{i}kx - \mathrm{i}\omega t) + \mathrm{c.c})$ be the disturbance of this interface between the clear fluid and the moving bed, with real wavenumber k and complex frequency ω. The important assumption here is that the moving bed velocity is so small that the shear stress exerted by the clear fluid on the moving bed is the same as if the bed were fixed. This assumption is valid if the moving bed velocity, of order $V_S\Theta^2 \sim \gamma d\Theta$, is very small compared to the fluid velocity $\gamma\delta$ at the penetration height δ of the vorticity disturbances. For Θ of order one, this assumption is equivalent to $\delta \gg d$, which is also a necessary condition for the moving bed to be considered as a continuum; it is satisfied for fluid thickness h, wavelength $2\pi/k$ and viscous length l_v large compared to particle diameter d. The latter condition $l_v \gg d$ is equivalent to $(kdRe_p)^{1/3} \ll 1$, which is satisfied for small kd and Re_p. Under these conditions, the shear stress disturbance exerted by the clear fluid on the moving bed is given by (3),

† The threshold $\Theta_t \approx 0.26$ was determined from two types of particles in mixtures of glycerine and water: Mississipi sediment ($d \approx 0.4$ mm, $Ga \approx 0.055$, $Re_p \approx 0.014$) and glass spheres ($d = 0.139$ mm, $Ga \approx 0.008$, $Re_p \approx 0.002$).

and corresponds to the Shields number disturbance:

$$\hat{\theta} = \frac{\hat{\tau}_b}{(\rho_p - \rho)gd} = -\Theta \frac{\hat{\tau}_b}{\mu\gamma}. \tag{16}$$

On the other hand, the threshold Shields number Θ_t is modified to $\Theta_t + \theta_t$ by the gravitational component parallel to the slope $\partial_x \eta$. For small slopes, the following expression gives good agreement with experiments with sand and water (Fredsøe & Deigaard 1992; Soulsby & Whitehouse 1997):

$$\frac{\theta_t}{\Theta_t} = \frac{\partial_x \eta}{\tan\chi} \quad \text{or} \quad \hat{\theta}_t = \frac{\Theta_t}{\tan\chi} \mathrm{i}k\hat{\eta}, \tag{17}$$

where χ is the static friction angle of the particles (angle of repose), and is typically about 32° (Bagnold 1973). We assume here that (17) still holds for viscous flow, with $\Theta_t/\tan\chi = 0.2/\tan 32° \approx 0.32$.

As shown in the next section, the instability time scale is much longer than the resuspension/sedimentation time scale $h_m/V_S \sim \Theta^2/\gamma$. Thus, the concentration and velocity profiles in the moving bed (see (B 5) and (B 6) in Appendix B) remain in equilibrium with the instantaneous shear stress, and the particle transport rate (15) can be used for the perturbed flow. Then, linearizing (15), the particle transport disturbance $\hat{q}\exp[\mathrm{i}(kx - \omega t)]$ in the moving bed yields

$$\frac{\hat{q}}{V_S d} = 3C(\Theta - \Theta_t)^2(\hat{\theta} - \hat{\theta}_t), \tag{18}$$

with $\hat{\theta}$ and $\hat{\theta}_t$ given by (16) and (17), respectively.

4. Wave velocity and growth rate

The time variation $\partial_t \eta$ of the interface position, and thus the wave velocity and growth rate of the instability, can be related to the particle transport gradient $\partial_x Q$ from the conservation of the number of particles. Within the quasi-static assumptions discussed in § 3.3 (small moving bed velocity and small growth rate), any negative (positive) particle transport gradient $\partial_x Q$ induces a local particle deposit (removal) which shifts the moving bed upwards (downwards), according to

$$\phi_0 \partial_t \eta + \partial_x Q = 0. \tag{19}$$

From this equation, the wave velocity $c = \omega_r/k$ and growth rate $\sigma = \omega_i$ are found to be

$$c = \frac{1}{\phi_0}\frac{\hat{q}_r}{\hat{\eta}}, \quad \sigma = \frac{1}{\phi_0}\frac{k\hat{q}_i}{\hat{\eta}}, \tag{20}$$

or, finally, together with (18),

$$\frac{c}{\gamma d} = K(\Theta - \Theta_t)^2 kd \frac{\hat{\tau}_{br}}{\mu\gamma k\hat{\eta}}, \tag{21}$$

$$\frac{\sigma}{\gamma} = K(\Theta - \Theta_t)^2 (kd)^2 \left\{ \frac{\hat{\tau}_{bi}}{\mu\gamma k\hat{\eta}} - \frac{\Theta_t}{\Theta \tan\chi} \right\}, \tag{22}$$

where $K = C/6\phi_0 \approx 2.16$, and the bed shear stress $\hat{\tau}_b = \hat{\tau}_{br} + \mathrm{i}\hat{\tau}_{bi}$ is given by (3). The above equations for the wave velocity and growth rate, with explicit dependence on the parameters, are the main results of this study. They show that the bed shear stress component in phase with the bed disturbance is responsible for the wave velocity,

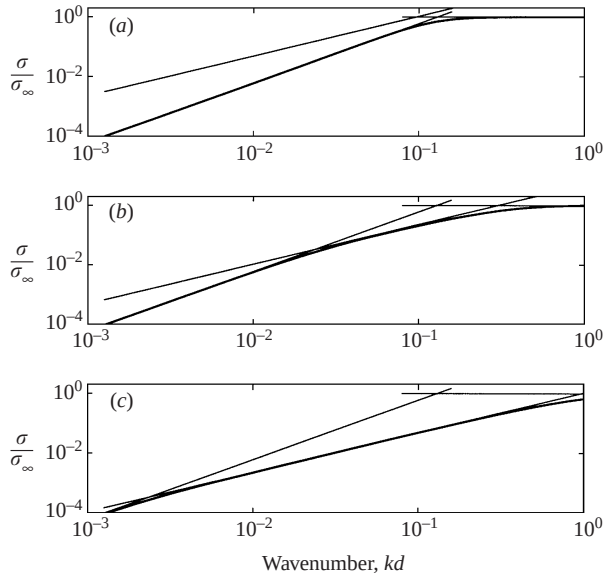

FIGURE 8. Normalized growth rate σ/σ_∞, with $\sigma_\infty = \sigma(k = \infty) = \frac{1}{2}\gamma K\, Ga\Theta(\Theta - \Theta_t)^2$; $h/d = 30$, $\Theta_t/\tan\chi = 0$. Straight lines correspond to the asymptotic regimes given by equation (23). (*a*) $Re_p = 0.01$, (*b*) $Re_p = 0.1$, (*c*) $Re_p = 1$.

whereas the out-of-phase component is responsible for the instability, because it drags the particles from the troughs to the crests of the bed disturbance. The bed shear stress depends only on the dimensionless thickness kh and viscous length kl_v, so that the wave velocity and growth rate depend on the four parameters Θ, kd, kh and kl_v (for given K, Θ_t and χ). However, rather than keeping this set of parameters, the predictions of equations (21) and (22) will be more conveniently discussed with the parameter set Θ, kd, h/d and Ga, where Ga is the Galileo number (10).

The expressions for the growth rate in the three asymptotic regimes can easily be obtained from (22) with (4)–(6):

shallow viscous regime

$$\frac{\sigma}{\gamma} = K(\Theta - \Theta_t)^2(kd)^2\left\{\frac{1}{30}\frac{h^2}{d^2}Ga\Theta - \frac{\Theta_t}{\Theta\tan\chi}\right\}, \tag{23a}$$

deep viscous regime

$$\frac{\sigma}{\gamma} = K(\Theta - \Theta_t)^2\left\{\tfrac{1}{2}Ga\Theta - (kd)^2\frac{\Theta_t}{\Theta\tan\chi}\right\}, \tag{23b}$$

boundary layer regime

$$\frac{\sigma}{\gamma} = K(\Theta - \Theta_t)^2\left\{\frac{1.06}{2}(kd)^{4/3}(Ga\Theta)^{1/3} - (kd)^2\frac{\Theta_t}{\Theta\tan\chi}\right\}, \tag{23c}$$

with similar expressions for the wave velocity.

First consider the case when the stabilizing effect of gravity is ignored ($\Theta_t/\tan\chi = 0$). In this case, the growth rate no longer depends on the particle diameter, but we retain it as the wavelength scale for easier comparison with what follows. Figure 8 displays the normalized growth rates $\sigma/\sigma(k = \infty)$ versus the dimensionless wavenumber kd, for fluid thickness $h/d = 30$ and three particle Reynolds

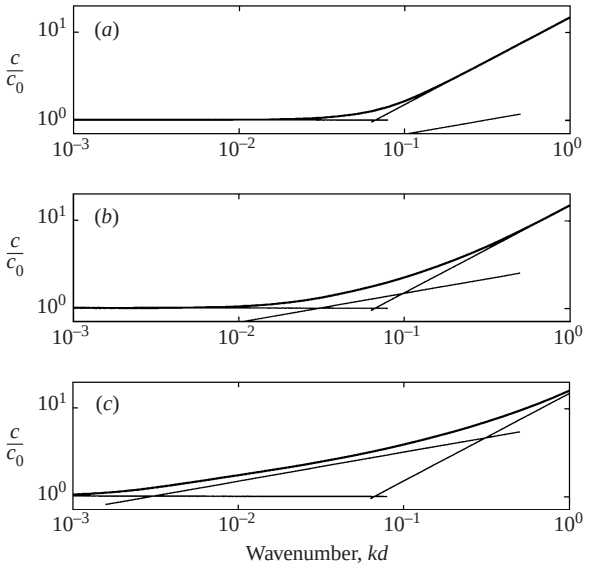

FIGURE 9. Normalized wave velocity c/c_0, with $c_0 = c(k=0) = \gamma d(4d/h)K\, Ga\Theta(\Theta - \Theta_t)^2$; $h/d = 30$, $\Theta_t/\tan\chi = 0$. Straight lines correspond to the asymptotic regimes. (a) $Re_p = 0.01$, (b) $Re_p = 0.1$, (c) $Re_p = 1$.

numbers $Re_p = Ga\Theta$. The chosen wavenumber range includes the longest ripples that can be expected, $\lambda/d \approx 2000$ (Raudkivi 1997; Yalin 1985), up to $kd = 1$ above which the long-wave assumption breaks down (see § 3.3), as well as the continuum description of the moving bed. It appears that the growth rate always increases monotically with wavenumber. For small Reynolds numbers (figure 8a, $Re_p = 0.01$), long waves are in the shallow viscous regime, with the growth rate scaling as k^2, whereas short waves are in the deep viscous regime, with constant growth rate. For higher Reynolds number (figure 8b, $Re_p = 0.1$), an intermediate range arises, corresponding to waves in the boundary layer regime, and the growth rate scaling as $k^{4/3}$. This boundary layer regime spreads as the Reynolds number is increased (figure 8c, $Re_p = 1$). The instability time scale σ^{-1} appears to be about $10^3/\gamma/Ga$. For the quasi-static assumption to be valid (see § 3.3), this time scale must much longer than the relaxation time Θ^2/γ of the moving bed. This condition is equivalent to $Ga\Theta^2 \ll 10^3$, which is satisfied for Θ of order one and small Ga. Figure 9 displays the corresponding wave velocity: it is constant in the shallow viscous regime (long waves are not dispersive), it scales as $k^{1/3}$ in the boundary layer regime, and as k in the deep viscous regime.

Inclusion of the gravity term, which scales as $-k^2$, stabilizes high wavenumbers. Figure 10 displays the normalized growth rate $\sigma/\gamma/Ga$ for fluid thickness $h/d = 30$, and Shields and Galileo numbers spanning a range of realistic situations (table 1). For $Ga = 0.1$ (figure 10a), all wavenumbers are stable for $\Theta/\Theta_t = 1.5$. For $\Theta/\Theta_t = 1.7$ and 1.8, long waves are unstable. The onset of instability corresponds to a change of the curvature of the growth rate curve for long waves (23a); this change occurs for equal inertia and gravity forces, at the critical Shields number Θ_c defined by

$$\frac{\Theta_c}{\Theta_t} = \left\{ \frac{30}{\Theta_t Ga \tan\chi} \right\}^{1/2} \frac{d}{h}. \tag{24}$$

For the parameters of figure 10(a), $\Theta_c \approx 1.65\Theta_t$. Thus, for $\Theta < \Theta_t$, the bed is at

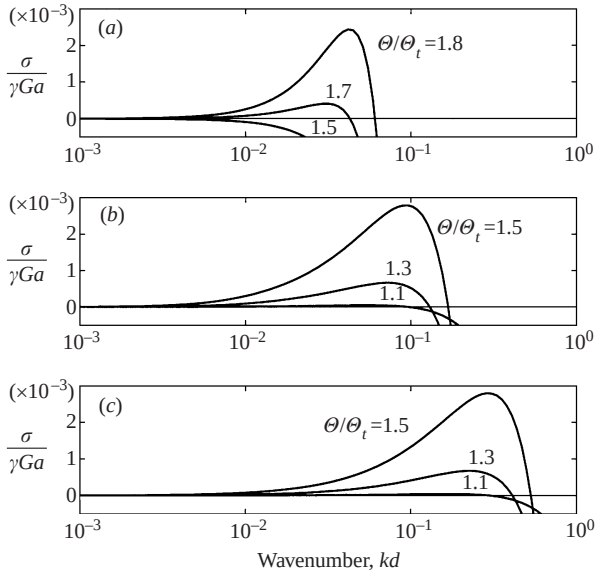

FIGURE 10. Normalized growth rate $\sigma/\gamma/Ga$ for three values of the Galileo number: (*a*) $Ga = 0.1$, (*b*) $Ga = 1$, (*c*) $Ga = 10$. Each curve is labelled with the corresponding Shields number. $\Theta_t/\tan\chi = 0.32$, $h/d = 30$. The corresponding shear Reynolds numbers are (*a*) $Re = 27$, 30.6, 32.4; (*b*) $Re = 198$, 234, 270; (*c*) $Re = 1980$, 2340, 2700.

rest; for $\Theta_t < \Theta < \Theta_c$, the moving bed is stable; and for $\Theta > \Theta_c$, the moving bed is unstable to long waves. It can be seen from (24) that for increasing Galileo number Ga or fluid thickness h/d, the critical Shields number Θ_c decreases. Thus, if the Galileo number or the fluid thickness are such that $\Theta_c/\Theta_t \leqslant 1$, the range $\Theta_t < \Theta < \Theta_c$ for which the moving flat bed is stable no longer exists; long waves are unstable as soon as particles move, i.e. as soon as $\Theta = \Theta_t$ (for $h/d = 30$, such a situation occurs when $Ga > 0.27$). The latter situation is illustrated in figure 10(*b*) ($Ga = 1$) and figure 10(*c*) ($Ga = 10$). (Note that in these two figures, the growth rate for $\Theta/\Theta_t = 1.1$, although small, is positive for wavenumbers below the cutoff wavenumber k_{off}.) Figure 10 also shows that the width of the unstable band, as well as the most unstable wavenumber, increase for increasing Shields number or Galileo number.

In fact, the existence of a stable moving bed depends on the value of the shear Reynolds number Re at the threshold Shields number Θ_t. Indeed, equation (24) can also be written

$$\frac{\Theta_c}{\Theta_t} = \left\{ \frac{30}{Re(\Theta_t)\tan\chi} \right\}^{1/2}.$$

This equation shows that if $Re(\Theta_t) < 30/\tan\chi \approx 48$, then $\Theta_c/\Theta_t > 1$, and there exists a range of stable Shields number; otherwise long waves are unstable as soon as particles move. Figures 10(*a*), 10(*b*) and 10(*c*) correspond to $Re(\Theta_t) = 18$, 180 and 1800, respectively. Physically interpreted, the existence of a stable moving bed originates in the stabilizing effect of the proximity of the upper plate, which reduces inertia effects for the long waves, and thus reduces the out-of-phase bed shear stress disturbance.

The cutoff wavenumber k_{off} ($\sigma = 0$), the wavenumber with maximum growth rate k_{max}, and the corresponding growth rate $\sigma_{max} = \sigma(k_{max})$ can be estimated as follows. The growth rate $\sigma(k)$ increases in the shallow viscous regime, and then decreases in

the boundary layer regime because the stabilizing effect of gravity, which scales as $-k^2$, is stronger than the destabilizing effect of inertia, which scales as $k^{4/3}$. Thus, for moderate Shields numbers, k_{off} and k_{max} are expected to be in the boundary layer regime, and can be estimated from (23*c*), giving

$$k_{off}d \approx \left(\frac{1.06}{2\Theta_t/\tan\chi}\right)^{3/2} Ga^{1/2}\Theta^2, \tag{25}$$

$$k_{max}d \approx \left(\frac{2}{3}\right)^{3/2} k_{off}d, \tag{26}$$

$$\frac{\sigma_{max}}{\gamma} \approx K(\Theta-\Theta_t)^2 \frac{1.06^3}{54(\Theta_t/\tan\chi)^2} Ga\Theta. \tag{27}$$

Note that the above quantities do not involve the fluid thickness. In order to compare, in the next section, the most amplified wavenumber (26) with experiments, it is useful to write (26) slightly differently with $Re_p = Ga\Theta$:

$$k_{max}d \approx \left(\frac{1.06}{2/\tan\chi}\right)^{3/2} \left(\frac{\Theta}{\Theta_t}\right)^{3/2} Re_p^{1/2}.$$

Thus, when the flat bed is unstable at the threshold Shields number Θ_t, the most amplified wavenumber at threshold is, with $\chi = 32^\circ$,

$$k_{max}d \approx 0.104 Re_p^{1/2} \quad \text{or} \quad \lambda_{max}/d \approx 60 Re_p^{-1/2}. \tag{28}$$

Thus, the most amplified wavelength $\lambda_{max} \approx 60(\nu/\gamma)^{1/2}$ scales with the viscous length $(\nu/\gamma)^{1/2} = \nu/u_*$. Introducing the penetration height $\delta = l_v$ of vorticity disturbances, one obtains $\lambda_{max} \approx 29 l_v$.

For high Shields numbers, the cutoff wavenumber is in the deep viscous regime, and can be estimated using (23*b*), yielding

$$k_{off}d \approx \left(\frac{Ga}{2\Theta_t/\tan\chi}\right)^{1/2} \Theta. \tag{29}$$

The Shields number beyond which the cutoff wavenumber can be estimated by (29) rather than by (25) corresponds to the crossing of the curves $k_{off}d(\Theta)$ given by (25) and (29), which leads to $\Theta = 2\Theta_t/\tan\chi/1.06^{3/2} \approx 0.59$.

The above results are summarized in the stability diagrams shown in figure 11 and figure 12. Figure 11 displays marginal stability curves obtained from (22) for a fixed Galileo number $Ga = 0.27$ and four fluid thicknesses h/d, as well as the estimated curves obtained from (25) and (29) (straight lines). This diagram clearly shows that when $h/d < 30$, there exists a range of stable Shields numbers (see marginal stability curves for $h/d = 10$ and 20), whereas this range no longer exists when $h/d > 30$ (see the curve for $h/d = 50$). Figure 12 displays the same marginal stability curves, for fixed thickness $h/d = 30$ and five Galileo numbers. For $Ga < 0.27$, there exists a range of Shields numbers for which the bed is moving and is stable (e.g. $Ga = 0.03$ and 0.1); for $Ga > 0.27$ this stable range no longer exists ($Ga = 1$ and 3).

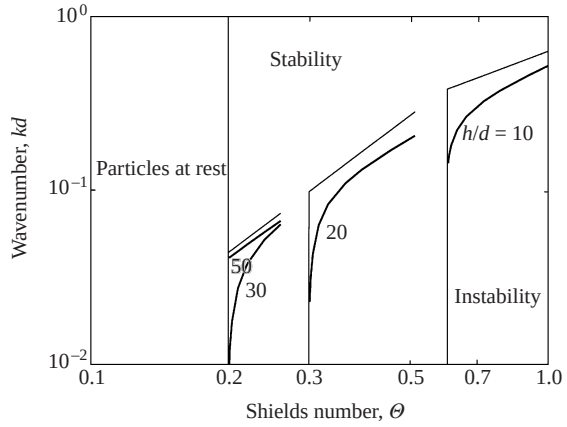

FIGURE 11. Marginal stability curves for $Ga = 0.27$ and four thicknesses h/d. Straight lines correspond to the estimated cutoff wavenumbers (25) and (29).

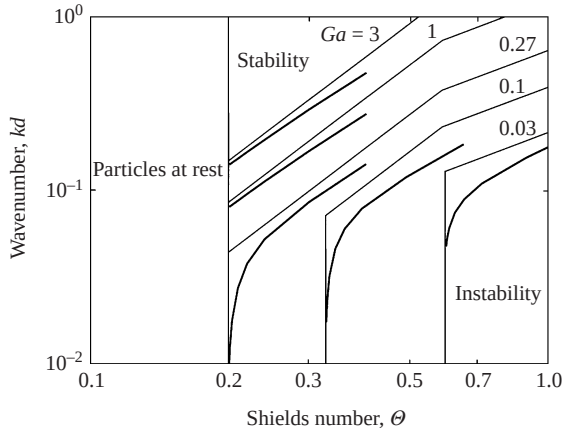

FIGURE 12. Marginal stability curves for five Galileo numbers and $h/d = 30$. Straight lines correspond to the estimated cutoff wavenumbers (25) and (29).

5. Discussion and conclusion

5.1. *Summary of results*

In this paper a simple analytical model has been presented for the instability of a bed of particles sheared by a viscous fluid for Shields number Θ (dimensionless bottom shear stress) of order one, which gives explicit expressions for the wave velocity and the growth rate (equations (21), (22)). The model involves three main assumptions. The first one is that the particle Reynolds number is small ($Re_p < 1$), for the viscous resuspension theory of Leighton & Acrivos to be valid. The second one is that the characteristic velocity $\Theta^2 V_S$ in the moving bed is small compared to the fluid velocity $\gamma\delta$ (at the penetration height δ of the vorticity disturbances induced by the wavy bed), so that the disturbance flow in the clear fluid can be calculated as if the bed were fixed. This assumption only requires that the particle diameter be small compared to the three length scales h, k^{-1} and l_v, the latter condition ($d \ll l_v$) being satisfied for small Re_p. The third assumption is that the relaxation time h_m/V_S of the bed is small compared to the instability time scale σ^{-1}. This assumption appears *a posteriori* to be satisfied if $Ga\Theta^2 \ll 10^3$, which is the case for small Galileo number.

Within this model, the instability mechanism is the following. The disturbance flow in the clear fluid creates a bed shear stress $\hat{\tau}_b \sim -\mu\hat{\omega}$ in phase with the bed disturbance, which drags the bed according to (18) and propagates the bed disturbance with the wave velocity (21). Long-wave instability arises from inertia effects in the clear fluid which shift the bed shear stress maximum upstream of the bed crest, according to the physical mechanism described in § 2. The out-of-phase bed shear stress component drives the particles from the bed troughs towards the crests, leading to the growth rate (22). Short waves are stabilized by gravity. Note that this instability is similar to that of the thin liquid layer sheared by a less viscous fluid, as described by Charru & Hinch (2000).

Two quite different situations may occur. On the one hand, for small enough fluid thickness (typically a few tens particle diameters), the moving bed is stable for Shields numbers in the range $\Theta_t < \Theta < \Theta_c$ (equation (24)); there, the closeness of the upper plate reduces inertia effects and all wavenumbers are stabilized by gravity. For $\Theta > \Theta_c$, wavenumbers smaller than a cutoff wavenumber k_{off} are unstable. On the other hand, for large fluid thickness, Θ_c is smaller than Θ_t, so that the bed is unstable as soon as particles move. The cutoff wavenumber k_{off}, as well as the most amplified wavenumber k_{max} and the corresponding growth rate σ_{max}, increase with increasing Shields number. Approximate expressions have been derived for these quantities: close to the threshold, the approximate cutoff wavenumber is given by (25); for Shields numbers higher than 0.59, it is given by (29).

5.2. *Sensitivity to the particle transport rate models*

We now briefly investigate the robustness of our results as a function of the different existing formulas for the particle transport rate versus shear stress. The above results were derived with the particle transport formula (13) obtained from the viscous resuspension theory of Leighton & Acrivos (1986) in which the threshold for particle transport Θ_t was introduced by analogy with the Meyer-Peter & Müller formula (equation (15)). A more general particle transport formula $Q/V_S d = C(\Theta - \Theta_t)^m$ would lead to essentially the same results, for any $m > 1$. In particular, the critical Shields number (24), the cutoff wavenumber (25) and (29), and the most unstable wavenumber (26) would remain unchanged, as well as the stability diagrams shown in figure 11 and figure 12. Another possibility, by analogy with the sediment transport formula proposed by Bagnold (1956), would be the slightly different expression $Q/V_S d = C\Theta^2(\Theta - \Theta_t)$. Again, the results are essentially the same, as can be seen in Appendix C. It may thus be concluded that the main results of the present study are largely independent of the existing particle transport formulas.

5.3. *Comparison with previous work*

The predictions of the present study can be compared with the stability analysis by Sumer & Bakioglu (1984), who extended the work of Richards (1980) for a turbulent flow over an erodible bed to an hydraulically smooth bed. It is remarkable that these two studies qualitatively predict the same results as ours: long-wave instability due to the bed shear stress component in phase with the slope of the wavy bed, and short waves stabilized by gravity effects proportional to $-k^2$. In particular, Sumer & Bakioglu show that for small particle Reynolds numbers, the most amplified wavenumber as well as the width of the unstable band scale with the viscous length ν/u_*, in agreement with the present study (see equation (28)). More precisely,

extrapolating their results to the viscous case,† their most amplified wavelength is found to be $\lambda_{max} \approx 17\nu/u_*$, whereas the present study predicts $\lambda_{max} \approx 60\nu/u_*$. Moreover, from their figures 5 and 7, the ratio k_{max}/k_{off} is found to be 0.57, which is very close to the ratio $(2/3)^{3/2} \approx 0.544$ predicted here.

We now turn to a comparison of the predictions of the present study with experiments. Equation (24) for the threshold, as well as equations (26) and (27) for the most amplified wavenumber and the corresponding growth rate might be expected to be easily tested. Unfortunately, no detailed experimental study was found to be available. Only wavelengths have been reported and no linear growth rates appear to have been measured. Two Couette flow experiments in annular channels have been performed, by Leighton & Acrivos (1986) and Betat, Frette & Rehberg (1999). Leighton & Acrivos (1986) measured the resuspension height for several types of particles and viscous fluids, but they do not report instabilities; the reason might be that their flows were in the stable range $\Theta_t < \Theta < \Theta_c$. Indeed, their Galileo number was in the range 10^{-6}–0.054, which gives $5 < \Theta_c/\Theta_t < 120$ for fluid thickness $h = 5\,\mathrm{mm}$. Betat *et al.* (1999) report strong ripples for glass beads in water ($Ga \approx 330$), with a wavelength $\lambda/d \approx 300$. However, their shear Reynolds number is about 6000, and the water flow is probably turbulent, so that the present study is not relevant.‡

Although the results of the present study are derived for Couette flow, they are expected to be valid for other flows such as Poiseuille or boundary layer flows provided the penetration height of the vorticity disturbances induced by the ripples is smaller than the height within which the shear rate is approximately constant. Therefore, our predictions can be compared with a number of additional experiments. Schaflinger *et al.* (1995) measured the pressure drop in plane Poiseuille flow of polystyrene beads in a water–ethanol mixture ($Ga \approx 5.0$). For $Ga = 5.0$ and $\Theta \approx 1$ (rough estimate), instabilities are reported at $\lambda/d \approx 54$ whereas our prediction (28) yields $\lambda/d \approx 27$. The difference could be attributed to the high particle Reynolds number, $Re_p \approx 5$. The convective nature of the instability might be responsible for the fact that it was not observed at smaller Shields numbers (i.e. it would have been observed in longer channels). Kuru *et al.* (1995) report ripple formation in Poiseuille pipe flow (glass beads and water–glycerin mixture). For their smallest Reynolds number which corresponds to laminar flow ($Ga \approx 20$, $\Theta \approx 0.10$ and $Re_p \approx 2.1$), the ripple length is $\lambda/d \approx 97$ and our prediction is $\lambda/d \approx 41$. However, their wavelengths increase with the friction velocity, which confirms that flow conditions are again too strong for the present theory to be truly applicable.

In contrast with the small number of resuspension flow experiments, the formation and growth of sand ripples in water flowing down inclined open channels has been extensively studied. However, for most data, grain inertia is not negligible, and only the experiments of Mantz (1978) and Yalin (1985) at small particle Reynolds numbers are relevant here. The data collected by Yalin (1977, 1985) show that for $Re_* < 2.5$ the ripple length would be $\lambda \approx 2200\nu/u_*$ and would scale with the thickness $\delta \approx 11.6\nu/u_*$

† The most amplified wavenumber of Sumer & Bakioglu (1984) depends on a parameter $\beta = 1/\tan\alpha$, where α is the dynamic friction angle introduced by Bagnold (1954). Extrapolating the results shown in their figure 7 to the case $\beta = 1.3$, which corresponds to the macro-viscous regime defined by Bagnold (1954), one finds $k_{max}\nu/u_* \approx 0.36$, i.e. $\lambda_{max} \approx 17\nu/u_*$.

‡ Betat *et al.* (1999) gives $Re_{*c} \approx 2.4$ as the critical particle Reynolds number for the appearance of ripples. However, this calculation is based on the hypothesis of linear shear flow, which probably underestimates particle Reynolds numbers. Indeed, for $Ga = 330$ in their experiments, taking the low value $\Theta_t = 0.04$ gives a particle Reynolds number at threshold for particle transport $Re_{*t} = (\Theta_t Ga)^{1/2} \approx 3.6$, so that particles should be at rest for $Re_{*c} \approx 2.4$.

of the viscous sublayer.† The two-dimensional ripples reported by Mantz (1978) correspond to $\lambda \approx 530\nu/u_*$.‡ Our result, $\lambda_{max} \approx 60\nu/u_*$, is in qualitative agreement with these observations, but it underpredicts the ripple length.

5.4. *Conclusion*

Many authors, e.g. Raudkivi (1997), have stated that our understanding of ripple formation remains unsatisfactory, in particular the basic comparison of linear stability results and experiments. The present study aimed at improving this understanding by the derivation of a viscous flow model which provides explicit expressions for the growth rate and wave velocity against all parameters. Unfortunately, appropriate experimental results for validation are still lacking. The ripple length reported in most experimental studies is in fact an 'equilibrium length' reached after a long coalescence process, which may be several times longer than the primary wavelet (Coleman & Melville 1994; Mantz 1978; Raudkivi 1997). Moreover, the results from classical flume experiments close to the threshold Shields number are doubtful: first, they involve small fluid thicknesses of a few centimetres, which could trigger resonant interaction between the bed and the free surface (such a resonance mechanism has been studied for inviscid potential flow by Coleman & Fenton 2000). Secondly, nonlinear effects may appear very soon: ripple growth increases the shear stress, and modifies the whole flow (Mantz 1978). Thus, well-controlled and well-designed experiments are highly desirable. Such experiments should investigate the early stages of the growth of ripples close to the threshold Shields number. These experiments should also elucidate the subcritical or supercritical nature of the instability as well as its convective or absolute character.

In parallel with such experiments, stability analysis still need to be refined by including a stronger coupling between the fluid flow and the bed as well as grain inertia (in our model as well as in all previous ones, the two-phase nature of the bed is accounted for only in the particle transport rate). As a next step, nonlinear theoretical studies, based on firm ideas on the linear instability mechanism, are then needed to understand the saturation of the ripple amplitude, its long-time evolution, as well as ripple coalescence. The long-wave instability predicted by the present model may appear to be a good starting point for such a nonlinear study. Indeed, weakly nonlinear analysis of long-wave instability (with the band of unstable wavenumbers including zero) has been shown to lead to wave coalescence and an increase of the wave height, e.g. Chang *et al.* (1997).

We thank Olivier Eiff for fruitful discussions and careful reading of this paper.

† The ripple length measured by Coleman & Melville (1996) seems to scale with the grain diameter, $\lambda/d \approx 200$, rather than with a viscous length. However, these ripples correspond to high particle Reynolds numbers, $Re_* \approx 4$ to 8 ($Ga = 140$). Within this range, the data collected by Yalin (1985) indicate that the equilibrium ripple length no longer scales with ν/u_* but reaches a flat minimum which, for $Ga = 140$, is about $\lambda/d \approx 650$.

‡ The two-dimensional ripples shown by Mantz in his figure 2(d) correspond to silica grains with diameter $d = 15\,\mu$m in water, so that $Ga = 0.054$. The ripple length is $\lambda \approx 50$ mm, and flow conditions correspond to $Re_* = 0.16$ and $\Theta = 0.46$, with $\Theta_t = 0.23$. According to the present study, these ripples are in the 'boundary layer' regime, and the penetration depth of vorticity disturbances is $l_v \approx 0.4$ mm. This penetration depth is smaller than the thickness of the viscous sublayer $11.6\nu/u_* \approx 1.1$ mm, so that the present study should be relevant.

Appendix A

The integration constants in (2) are given by

$$C_1(kh, kl_v) = \frac{B^+ - B^-}{A^+B^- - A^-B^+}, \quad C_2(kh, kl_v) = -\frac{A^+ - A^-}{A^+B^- - A^-B^+}, \tag{A 1}$$

with

$$A^\pm = \int_0^{kh} \mathrm{e}^{\pm Y} \mathrm{Ai}(z(Y))\,\mathrm{d}Y, \quad B^\pm = \int_0^{kh} \mathrm{e}^{\pm Y} \mathrm{Bi}(z(Y))\,\mathrm{d}Y,$$

and

$$z(Y) = \frac{1}{kl_v}(Y - \mathrm{i}(kl_v)^3)\mathrm{e}^{\mathrm{i}\pi/6},$$

and the streamfunction is given by

$$\frac{k^2}{\gamma}\hat{\Psi}(y) = \frac{1}{2}\left\{\mathrm{e}^{-ky}\int_0^{ky} \mathrm{e}^{Y}\hat{\omega}(Y)\,\mathrm{d}Y + \mathrm{e}^{ky}\int_{ky}^{kh} \mathrm{e}^{-Y}\hat{\omega}(Y)\,\mathrm{d}Y\right\} + \tfrac{1}{2}\mathrm{e}^{-ky}. \tag{A 2}$$

Appendix B

This Appendix summarizes the viscous resuspension theory of Leighton & Acrivos (1986). The origin of the vertical y-axis here is set at the location of the interface at rest, as in their paper. The mixture is assumed to behave as a Newtonian fluid with density $\rho(\phi)$ and effective viscosity $\mu_r(\phi)\mu$, where $\mu_r(\phi)$ is the relative viscosity ($\mu_r = 1$ for the pure fluid). For a pure shearing flow, integrating the x-momentum conservation equation, $\partial_y(\mu\partial_y U) = 0$, gives

$$\frac{1}{18}\mu_r \frac{\mathrm{d}U/V_S}{\mathrm{d}y/d} = \Theta, \tag{B 1}$$

where $V_S = (\rho_p - \rho)gd^2/18\mu$ is the Stokes settling velocity of a single sphere. The mass conservation of the particles expressing the equilibrium between downwards sedimentation and upwards diffusion, can be written as

$$f(\phi)V_S\phi + (\gamma d^2/4)D(\phi)\partial_y\phi = 0. \tag{B 2}$$

Here, the first term is the sedimentation flux, where $f(\phi)$ is the 'hindrance function' taking into account the retarding effect of the other spheres on the Stokes settling velocity. The second term is the shear-induced diffusion flux, where $D(\phi) = O(1)$ is the dimensionless diffusion coefficient (Leighton & Acrivos 1987). The empirical relations for $f(\phi)$, $\mu_r(\phi)$ and $D(\phi)$ proposed by Leighton & Acrivos (1986) are

$$f(\phi) = \frac{1-\phi}{\mu_r(\phi)}, \quad \mu_r(\phi) = \left(1 + \frac{1.5\phi}{1-\phi/\phi_0}\right)^2, \quad D(\phi) = \tfrac{1}{3}\phi^2(1 + \tfrac{1}{2}\exp(8.8\phi)), \tag{B 3a–c}$$

with $\phi_0 = 0.58$. Then, the upper and lower bounds of the resuspended layer at $y = h_u$ and $y = -h_l$, respectively, are found to be

$$\frac{h_u}{d} = \tfrac{9}{2}\Theta\int_0^{\phi_0}\left(\frac{1}{\phi} - \frac{1}{\phi_0}\right)\frac{D}{f\mu_r}\,\mathrm{d}\phi \approx 1.86\Theta, \tag{B 4a}$$

$$\frac{h_l}{d} = \tfrac{9}{2}\Theta\int_0^{\phi_0}\frac{1}{\phi_0}\frac{D}{f\mu_r}\,\mathrm{d}\phi \approx 11.8\Theta. \tag{B 4b}$$

The height y and velocity U at which the volume concentration is ϕ are given by

$$\frac{y+h_l}{d} = \tfrac{9}{2}\Theta \int_{\phi}^{\phi_0} \frac{1}{\phi}\frac{D}{f\mu_r}\,\mathrm{d}\phi, \tag{B 5}$$

$$\frac{U}{V_S} = 4(\tfrac{9}{2})^2\Theta^2 \int_{\phi}^{\phi_0} \frac{1}{\phi}\frac{D}{f\mu_r^2}\,\mathrm{d}\phi. \tag{B 6}$$

Finally, the particle flow rate is given by

$$\frac{Q}{V_S d} = \frac{1}{V_S d}\int_{-h_l}^{h_u} \phi U\,\mathrm{d}y = C\Theta^3, \tag{B 7}$$

with

$$C = 4(\tfrac{9}{2})^3 \int_0^{\phi_0} \left\{ \frac{D}{f\mu_r} \int_{\phi}^{\phi_0} \frac{1}{\phi}\frac{D}{f\mu_r^2}\,\mathrm{d}\phi \right\} \mathrm{d}\phi \approx 7.5.$$

Appendix C

By analogy with the sediment transport formula proposed by Bagnold (1956), the expression

$$\frac{Q}{V_S d} = C\Theta^2(\Theta - \Theta_t) \tag{C 1}$$

could also be used for the particle transport rate. The critical fluid thickness above which the bed is unstable as soon as particles move is still defined by (24) with $\Theta_c/\Theta_t = 1$. For smaller fluid thickness, the moving bed becomes unstable at the critical Shields number Θ_{c2} defined by

$$\frac{\Theta_{c2}}{\Theta_t} = \frac{1}{3}\left\{ 1 + \left\{ 1 + 3\frac{\Theta_c^2}{\Theta_t^2} \right\}^{1/2} \right\} \tag{C 2}$$

where Θ_c is given by (24). Thus, the range of stable Shields number is larger than that obtained from the particle transport formula (15). The band of unstable wavenumbers is also larger, by a factor $(3-2\Theta_t/\Theta)^{3/2}$ for $\Theta < 0.33$ and by a factor $(3-2\Theta_t/\Theta)^{1/2}$ for $\Theta > 0.33$.

REFERENCES

Bagnold, R. A. 1954 Experiments on a gravity-free dispersion of large solid spheres in a Newtonian fluid under shear. *Proc. R. Soc. Lond.* A **225**, 49–63.

Bagnold, R. A. 1956 The flow of cohesionless grains in fluids. *Phil. Trans. R. Soc. Lond.* A **249**, 235–297.

Bagnold, R. A. 1966 An approach to the sediment transport problem from general physics. *US Geol. Surv. Prof. Paper* **422-I**, 1–37.

Bagnold, R. A. 1973 The nature of saltation and of 'bed-load' transport in water. *Proc. R. Soc. Lond.* A **332**, 473–504.

Betat, A., Frette, V. & Rehberg, I. 1999 Sand ripples induced by water shear flow in an annular channel. *Phys. Rev. Lett.* **83**, 88–91.

Blondeaux, P. 1990 Sand ripples under sea waves. Part 1. Ripple formation. *J. Fluid Mech.* **218**, 1–17.

Chang, H.-C., Demekhin, E. A., Kopelevich, D. I. & Ye, Y. 1997 Nonlinear wavenumber selection in gradient flow systems. *Phys. Rev.* E **55**, 2818–2834.

Charru, F. & Hinch, E. J. 2000 'Phase diagram' of interfacial instabilites in a two-layer Couette flow and mechanism for the long-wave instability. *J. Fluid Mech.* **414**, 195–223.

Coleman, S. E. & Fenton, J. D. 2000 Potential-flow instability theory and alluvial stream bed forms. *J. Fluid Mech.* **418**, 101–117.

Coleman, S. E. & Melville, B. W. 1994 Bed-form development. *J. Hydr. Engng ASCE* **120**, 544–560.

Coleman, S. E. & Melville, B. W. 1996 Initiation of bed forms on a flat sand bed. *J. Hydr. Engng ASCE* **122**, 301–310.

Engelund, F. & Fredsøe, J. 1982 Sediment ripples and dunes. *Annu. Rev. Fluid Mech.* **14**, 13–37.

Fredsøe, J. & Deigaard, R. 1992 *Mechanics of Coastal Sediment Transport*. World Scientific.

Gadala-Maria, F. A. & Acrivos, A. 1980 Shear-induced structure in a concentrated suspension of solid spheres. *J. Rheol.* **24**, 799–814.

Hooper, A. P. & Boyd, W. G. C. 1983 Shear-flow instability at the interface between two viscous fluids. *J. Fluid Mech.* **128**, 507–528.

Kuru, W. C., Leighton, D. T. & McCready, M. J. 1995 Formation of waves on a horizontal erodible bed of particles. *Intl J. Multiphase Flow* **21**, 1123–1140.

Leighton, D. & Acrivos, A. 1986 Viscous resuspension. *Chem. Engng Sci.* **41**, 1377–1384.

Leighton, D. & Acrivos, A. 1987 The shear-induced migration of particles in concentrated suspensions. *J. Fluid Mech.* **181**, 415–439.

Loimer, T. & Schaflinger, U. 1998 The effect of interfacial instabilities in a stratified resuspension flow on the pressure loss. *Phys. Fluids* **10**, 2737–2745.

Mantz, P. A. 1977 Incipient transport of fine grains and flakes by fluids – Extended Shields diagram. *J. Hydr. Div. ASCE* **103**, 601–615.

Mantz, P. A. 1978 Bedforms produced by fine, cohesionless, granular and flakey sediments under subcritical water flows. *Sedimentology* **25**, 83–103.

Miskin, I., Elliott, L. & Ingham, D. B. 1999 Stability in a fully-developed two-dimensional resuspension flow. *Intl J. Multiphase Flow* **25**, 501–530.

Morris, J. F. & Brady, J. F. 1998 Pressure driven flow of a suspension: Buoyancy effects. *Intl J. Multiphase Flow* **24**, 105–130.

Phillips, R. J., Armstrong, R. C., Brown, R. A., Graham, A. L. & Abbott, J. R. 1992 A constitutive equation for concentrated suspensions that accounts for shear-induced particle migration. *Phys. Fluids* A **4**, 30–40.

Raudkivi, A. J. 1997 Ripples on stream bed. *J. Hydr. Engng ASCE* **123**, 58–64.

Raudkivi, A. J. 1998 *Loose Boundary Hydraulics*. A. A. Balkema, Rotterdam.

Richards, K. J. 1980 The formation of ripples and dunes on an erodible bed. *J. Fluid Mech.* **99**, 597–618.

Schaflinger, U. 1994 Interfacial instabilities in a stratified flow of two superposed fluids. *Fluid Dyn. Res.* **13**, 299–316.

Schaflinger, U., Acrivos, A. & Stibi, H. 1995 An experimental study of viscous resuspension in a pressure-driven plane channel flow. *Intl J. Multiphase Flow* **21**, 693–704.

Schaflinger, U., Acrivos, A. & Zhang, K. 1990 Viscous resuspension of a sediment within a laminar and stratified flow. *Intl J. Multiphase Flow* **16**, 567–578.

Soulsby, R. L. & Whitehouse, R. J. S. 1997 Threshold of sediment motion in coastal environments. In *Proc. Australasian Coastal Engng and Ports Conf., Christchurch*, pp. 149–154.

Sumer, B. M. & Bakioglu, M. 1984 On the formation of ripples on an erodible bed. *J. Fluid Mech.* **144**, 177–190.

Van Rijn, L. C. 1993 *Principles of Sediment Transport in Rivers, Estuaries and Coastal Seas*. Aqua Publications, Amsterdam.

White, C. M. 1940 The equilibrium of grains on the bed of a stream. *Proc. R. Soc. Lond.* A **174**, 322–338.

White, S. J. 1970 Plane bed thresholds of fine grained sediments. *Nature* **228**, 152–153.

Yalin, M. S. 1977 On the determination of ripple length. *J. Hydr. Engng ASCE* **103**, 439–442.

Yalin, M. S. 1985 On the determination of ripple geometry. *J. Hydr. Engng ASCE* **111**, 1148–1155.

Yalin, M. S. & Karahan, E. 1979 Inception of sediment transport. *J. Hydr. Div. ASCE* **105**, 1433–1443.

Yih, C. S. 1967 Instability due to viscous stratification. *J. Fluid Mech.* **27**, 337–352.

Zhang, K., Acrivos, A. & Shaflinger, U. 1992 Stability in a two-dimensional Hagen–Poiseuille resuspension flow. *Intl J. Multiphase Flow* **18**, 51–63.